7.14 A STOCHASTIC MODEL FOR TURBULENT VERTICAL TRANSPORT

Scott Wunsch and Alan R. Kerstein
Combustion Research Facility, Sandia National Laboratories, Livermore, California

Abstract

The One-Dimensional Turbulence (ODT) model is a single-column simulation in which vertical turbulent transport is modeled by an unsteady, stochastic advective process, rather than the customary representation by a diffusive process. Unlike conventional single-column models, ODT resolves small-scale, unsteady motions and transport processes in the atmospheric boundary layer. ODT has been validated against laboratory data for a number of different convective, stably-stratified, sheared, and reacting flow configurations. This paper summarizes the ODT approach and provides a survey of results relevant to atmospheric boundary layer modeling.

1 INTRODUCTION

One-Dimensional Turbulence (ODT) is a turbulence simulation model formulated on a one-dimensional (1D) spatial domain. Its roots lie in the Linear Eddy Model, or LEM (Kerstein, 1991), which was conceived as a computationally efficient way to model the mixing of passive scalars in a turbulent flow. LEM has previously been used to study turbulent mixing in clouds (Krueger, 1993, and Su, *et al.* 1998). ODT generalizes LEM by using ideas from mixing length theory to allow the scalar fields to self-consistently determine the rate of turbulent mixing in the model (Kerstein, 1999).

In the context of the atmospheric boundary layer (ABL), the ODT model functions as a single-column model (SCM). The 1D domain corresponds to a vertical column of air, and any number of scalar fields (such as potential temperature) may be defined on that domain. The unique characteristic of ODT, compared to most other SCMs, is that turbulent advection is implemented by non-local, instantaneous rearrangements of the vertical column, rather than by local, diffusive exchanges between neighboring fluid elements. The frequency of these rearrangement events depends on the current scalar field values in the model. For example, portions of the vertical column with a very unstable stratification will experience more frequent rearrangements than regions with a neutral or stable stratification. In addition to the rearrangement events, local diffusive mixing is also explicitly represented on the small length scales. Hence turbulent advection and physical diffusion are algorithmically distinct processes within the ODT model.

The non-local exchange of fluid between distant parts of the air column is reminiscent of Stull's (1988) transilient model. However, Stull's advection model only exchanges a fraction of the material between fluid elements in one time step, while ODT's advection algorithm utilizes complete exchanges to avoid any unphysical diffusive mixing. Also, in Stull's model all fluid elements are continuously exchanging fluid with distant elements, while in ODT only a fraction of the fluid elements in the air column are involved in any one rearrangement event.

In this work, the formulation of the ODT model for buoyant flows (applicable to both stable and unstable stratification) is presented, along with some previous comparisions to laboratory experiments and simplified ABL configurations. Ideas for future work in the ABL context are also discussed.

2 ODT MODEL OVERVIEW

In many cases, the buoyancy structure in the atmospheric boundary layer is primarily a function of the vertical coordinate z. Hence it is plausible that a one-dimensional, single-column model such as ODT might plausibly describe ABL physics in these cases. At a minimum, two scalar fields are necessary to describe the ABL flow in the ODT model. One is the potential temperature $\theta(z,t)$. The other is a velocity scalar, $w(z,t)$, which (when squared) represents a vertical profile of kinetic energy. It is not a real velocity in the sense that it does not directly advect itself or the potential temperature. Rather, it serves as a repository of kinetic energy in the model. This basic ODT formulation for buoyant

flows is described in greater detail, along with applications to different flow configurations, in Wunsch & Kerstein (2001); Wunsch (2003); and Wunsch & Kerstein (2004).

For ABL problems, it is advantageous to generalize the basic buoyant ODT formulation by splitting the single velocity scalar $w(z,t)$ into the three components of the physical velocity vector, $u(z,t)$, $v(z,t)$, and $w(z,t)$. The sum of the squares of these components still represents a kinetic energy, but this separation allows for the inclusion of geostrophic winds which drive only the horizontal velocity components. This variant of the ODT model is described here, and further details may be found in Kerstein & Wunsch (2004). Additional scalar fields representing other properties of interest (water vapor, for example) can easily be added to the ODT model.

In ODT, advection consists of randomly chosen, measure-preserving mapping events which rearrange the scalar fields. Each mapping is a local event, with a well-defined vertical position z_o and spatial extent l. Each is loosely interpreted as corresponding to a turbulent 'eddy' of size l in the ABL. The mapping function is designed to 'wrinkle' the flow, reducing length scales within the affected area. The times and locations of the mapping events are selected at random from a probability distribution function based on the energetics of turbulence. Essentially, the mappings mimic turbulent advection by having mappings at each length scale occur approximately once each eddy turnover time, so that, over many turnover times, the effects of the mappings approximate the effects of an ensemble of eddies in a real flow. During the time between these instantaneous mappings, the scalar fields evolve according to the molecular transport equations:

$$\left(\partial_t - \kappa\partial_z^2\right)\theta(z,t) = 0. \tag{1}$$

$$\left(\partial_t - \nu\partial_z^2\right)u(z,t) = f\left(v(z,t) - V_g\right) \tag{2}$$

$$\left(\partial_t - \nu\partial_z^2\right)v(z,t) = -f\left(u(z,t) - U_g\right) \tag{3}$$

$$\left(\partial_t - \nu\partial_z^2\right)w(z,t) = 0. \tag{4}$$

Here ν and κ are the viscosity and thermal diffusivity of air; U_g and V_g are specified geostrophic wind components, and f is the Coriolis parameter. These equations are solved within a closed domain of height Λ. The boundary conditions depend on the specific flow being studied. The equations are solved as a time-sequence of initial-value problems, each starting immediately after a mapping event and proceeding until the time of the next event. In the simpler, single velocity component formulation, the scalars $\theta(z,t)$ and $w(z,t)$ obey equations 1 and 4, respectively.

The novel element of the model is the advective mapping. It consists of a measure-preserving map $M(z)$ of the domain onto itself, so that any scalar $\psi(z)$ undergoes the transformation $\psi(z) \to \psi(M(z))$ when acted on by the map. Measure-preservation, the one-dimensional equivalent of incompressibility, implies conservation of all moments of any scalar field. The mapping acts on a segment of length l, from position z_o to $z_o + l$. It is loosely interpreted as representing the effects of an 'eddy' of size l on the scalar fields in that interval. The velocity components and potential temperature are all mapped to mimic the transport of fluid elements. The particular mapping function is arbitrary, but a piecewise-linear function is chosen as a convenient way to satisfy the requirements of measure-preservation and finite extent. As in all previous ODT work, a three-piece function which takes the line segment, shrinks it to a third of its original length, and then places three copies on the original domain, is used (Kerstein, 1999). The middle copy is reversed, so that the mapped field $\psi(M(z))$ is continuous if $\psi(z)$ is continuous. The mapping function reduces to the identity map $M(z) = z$ outside of the mapped interval.

The rearrangement of the potential temperature field by the mapping alters the total potential energy, but the mapping itself leaves the total kinetic energy unchanged. To enforce energy conservation, a function of specified form is added to the velocity components whenever an eddy mapping occurs. The fluid displacements induced by the mapping are $K(z) \equiv z - M(z)$; this is the natural candidate for the energy exchange function. This function is non-zero only within the mapped region. Under the action of an eddy mapping, the potential temperature and velocity fields undergo the transformations

$$\begin{aligned} \theta(z) &\to \theta(M(z)) \\ u(z) &\to u(M(z)) + c_u K(z) \\ v(z) &\to v(M(z)) + c_v K(z) \\ w(z) &\to w(M(z)) + c_w K(z). \end{aligned} \tag{5}$$

The amplitude c_i of the energy exchange terms $c_i K(z)$ is determined for each eddy mapping individually to achieve energy conservation. In

ODT, the energy per unit mass e is defined as

$$e \equiv \frac{1}{2\Lambda}\int \left(u^2(z)+v^2(z)+w^2(z)\right)dz + \frac{g\beta}{\Lambda}\int \theta(z) z dz \tag{6}$$

where g is the gravitational acceleration and β is the coefficient of thermal expansion. The requirement of energy conservation provides one constraint among the three coefficients c_i. (In the simpler buoyant flow model with only one velocity scalar, energy conservation alone is sufficient to determiine c_w and close the model). For three velocity components, a generalization of the equipartition model of Ashurst, *et al.* (2001) is applied, yielding

$$\begin{aligned} c_u &= \frac{27}{4l}\left(-u_K \pm D\right) \\ c_v &= \frac{27}{4l}\left(-v_K \pm D\right) \\ c_w &= \frac{27}{4l}\left(-w_K \pm D\right) \end{aligned} \tag{7}$$

where

$$D^2 \equiv \frac{1}{3}\left(u_K^2+v_K^2+w_K^2-\frac{8}{27}g\beta l\theta_K\right) \tag{8}$$

and

$$s_K \equiv \frac{4}{9l^2}\int_{z_o}^{z_o+l} s(z)(l-2(z-z_o))dz \tag{9}$$

is a function of any scalar profile s. Substitution of these constants into equation 5 verifies the conservation of energy.

The final ingredient required in the model is to determine the frequency with which a particular eddy, with position z_o and size l, should occur. To estimate a time scale for each eddy, consider the convective turnover time τ for eddies driven by an unstable potential temperature difference $\delta\theta$: $\tau \sim \sqrt{l/g\beta\delta\theta}$. In real turbulence, this is roughly the time required for a region of size l to mix convectively. In ODT, eddy mappings are randomly selected and instantaneously implemented, but occur approximately once each turnover time. Quantitatively, the effective potential temperature difference $\delta\theta$ across an eddy is determined in ODT by the potential energy change due to the implementation of the mapping. Although potential temperature differences are major drivers of eddy turnovers in these flows, kinetic energy is also important. The typical turnover time for eddies in the absence of potential temperature differences scales as $\tau(l) \sim l/\tilde{v}(l)$, where $\tilde{v}(l)$ is some measure of the velocity fluctuations. A convenient choice for $\tilde{v}(l)$ is v_K, which arose previously in the energy exchange mechanism. Both of these contributions (potential and kinetic energy) need to be combined to construct the complete eddy turnover time. While the precise functional form of the combination is arbitrary, we choose a linear combination for internal self-consistency with the ODT energy conservation mechanism (eq. 7):

$$\left(\frac{l}{\tau}\right)^2 \sim \left(u_K^2+v_K^2+w_K^2\right)-\frac{8}{27}g\beta l\theta_K - Z\frac{\nu^2}{l^2}. \tag{10}$$

Eddy mappings which give an imaginary value for τ are of course prohibited by energetic considerations. Hence eddies are prohibited in regions of stable potential temperature stratification ($\theta_K \geq 0$) unless there is sufficient kinetic energy to overturn the potential temperature profile. The last term in eq. 10 represents a form of viscous cut-off. Eddies of extremely small size should not occur, due to the damping effects of viscosity. Any eddy with a time scale much longer than the corresponding viscous time scale $\tau_\nu \sim l^2/\nu$ for that eddy size should be prohibited. The coefficient Z in this term is an order-unity parameter of the model.

The time scales τ for all possible eddies are translated into an eddy rate λ, defined as $\lambda(z_o,l;t) \equiv C/l^2\tau(z_o,l;t)$. All of the interesting physics is subsumed in τ (equation 10), except for a dimensionless constant C (a parameter of the model). Using the turnover time in equation 10, the eddy rate is given by

$$\lambda = \frac{C\nu}{l^4}\sqrt{\frac{(u_K^2+v_K^2+w_K^2)l^2}{\nu^2}-\frac{8g\beta}{27\nu^2}\theta_K l^3 - Z}. \tag{11}$$

Once can see that, in the absence of gravity, a 'local Reynolds number' determines the rate of each eddy. Buoyant forces either enhance or lower the effective local Reynolds number. The construction of the ODT eddy rate given above utilizes two arbitrary constants, C and Z. The overall rate constant C determines the strength of the turbulence in the model, while Z determines the Reynolds number threshold for eddy turnover.

3 COMPARISON WITH LAB EXPERIMENTS

To illustrate some of the aspects of buoyant flows relevant to the ABL that can be simulated in ODT, highlights from previous work are presented here. While most of these simulations use the simpler, single velocity scalar version of ODT, the results are not expected to differ significantly from the three-component version outlined in section two. Comparisons with experimental results are used to demonstrate the quantitative accuracy achievable with the model.

3.1 Rayleigh-Beńard Convection

While turbulent thermal convection has long been recognized as an important aspect of the ABL, the physics of thermal convection is most frequently studied in the laboratory using Rayleigh-Beńard systems, in which a cylinder of fluid is heated from below. The resulting temperature contrast in the fluid generates turbulent motions which transport heat from the lower plate to the upper plate of the cell. The long history of both experimental and theoretical investigations of this system are summarized in Siggia (1994) and Kadanoff (2001).

The strength of the buoyant forcing in Rayleigh-Beńard convection is given by the Rayleigh number, Ra, defined as

$$Ra \equiv \frac{g\beta\Lambda^3\Delta\theta}{\nu\kappa} \tag{12}$$

where $\Delta\theta$ is the potential temperature difference between the plates and Λ is their separation. Experimental studies of Rayleigh-Beńard systems typically focus on the dependence of the dimensionless rate of heat transfer, or Nusselt number (Nu), on the Rayleigh number and the Prandtl number, $Pr \equiv \nu/\kappa$. Some experiments also measure the potential temperature fluctuations in the core of the convection cell.

Extensive simulations of turbulent Rayleigh-Beńard convection, for a wide range of Ra and Pr, have been reported in Wunsch & Kerstein (2004). Figure 1 shows a typical potential temperature profile from one of those simulations. The variations in the instantaneous profile illustrate the ability of ODT to represent turbulent fluctuations, while the time-averaged profile is

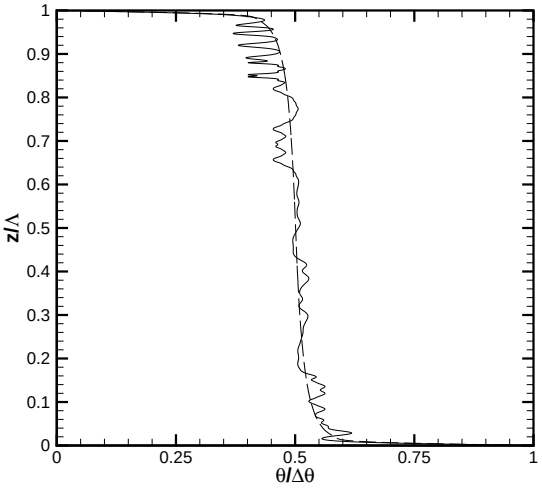

Figure 1: Typical ODT instantaneous (solid line) and time-averaged (dashed line) potential temperature profiles for Rayleigh-Beńard convection with $Ra = 10^8$ and $Pr = 0.7$.

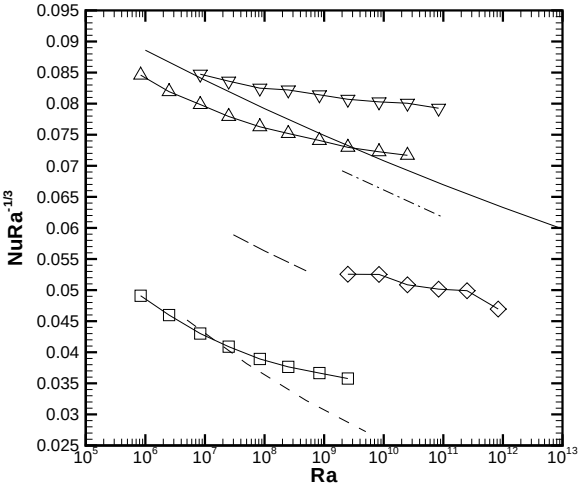

Figure 2: Nu as a function of Ra in Rayleigh-Beńard convection. Symbols are ODT simulation results for $Pr = 0.025$ (squares), $Pr = 0.7$ (Δ's), $Pr = 4$ (∇'s) and $Pr = 1352$ (diamonds). Lines are reported fits to experimental data for $Pr = 0.025$ from Cioni *et al.* (1997) (dashed line), $Pr = 0.7$ from Niemela *et al.* (2000) (solid line), $Pr = 4$ from Ahlers & Xu (2002) (dotted-dashed line), and $Pr = 1352$ from Xia *et al.* (2002) (long-dashed line).

used to compute average quantities like the Nusselt number Nu.

Figure 2 compares ODT results for Nu to experimental data in large-aspect ratio convection cells. The ODT model parameters were set to $ZC^2 = 10^4$ and $C^2 = 1200$ for this comparison. The ODT simulations shown cover a very wide range of parameter space: six orders of magnitude in Ra and five orders of magnitude in Pr. The results are plotted using $NuRa^{-1/3}$, which highlights deviations from classical scaling, since Nu itself varies by more than two orders of magnitude while $NuRa^{-1/3}$ varies only by a factor of three. The ODT data agree very well with the mercury ($Pr = 0.025$) convection data of Cioni *et al.* (1997), with the largest discrepancy being only about 15%. The $Pr = 0.7$ ODT results match the helium data of Niemela *et al.* (2000) to within 5%, and the high Prandtl number case plausibly matches the $Pr = 1352$ data of Xia *et al.* (2002), although the range of Rayleigh numbers do not overlap. However, the ODT Nu values for $Pr = 4$ consistently exceed those of Ahlers & Xu (2002) by about 25%.

The wide range of spatial and temporal scales present in the ODT simulations allows for the study of fluctuations in far greater detail than is possible with traditional SCMs. Figure 3 shows the scaling with Ra of the root-mean-square magnitude of the potential temperature fluctuations in the core of the cell for four different Pr. The data match the experimental measurements of Niemela *et al.* (2000) very well, but also exhibit different trends for other values of Pr.

The probability distribution function (PDF) of potential temperature fluctuations can also be examined using the ODT model. Figure 4 shows a comparison of the normalized shape of the PDF in ODT and in the experiment of Daya & Ecke (2001); the results are indistinguishable. Similar comparisons with the PDFs measured by Niemela *et al.* (2000) are also favorable.

These intercomparisons between the ODT model and experimental Rayleigh-Beńard convection data demonstrate the ODT model's ability to reproduce many relevant flow properties (heat transfer rates, fluctuation magnitudes, and PDF shapes) over a wide range of parameter space with only two adjustable parameters. Quantitative descrepancies between ODT results and experiments are typically about 10% in quantities that vary by orders of magnitude.

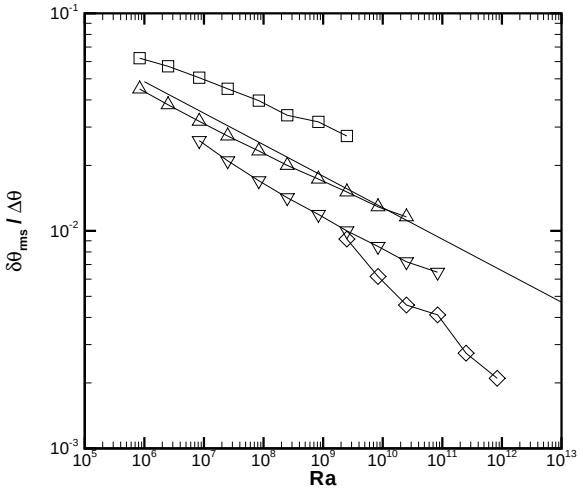

Figure 3: Magnitude of potential temperature fluctuations in the interior of a Rayleigh-Beńard cell. Symbols are ODT simulation results for $Pr = 0.025$ (squares), $Pr = 0.7$ (Δ's), $Pr = 4$ (∇'s) and $Pr = 1352$ (diamonds); the solid line is $\delta\theta_{rms}/\Delta\theta = 0.37Ra^{-0.145}$, a reported fit to $Pr = 0.7$ experimental data by Niemela *et al.* (2000).

3.2 Stably Stratified Turbulence

The same ODT model used to study Rayleigh-Beńard convection can also be applied to stably stratified turbulence. The only differences are that the vertical potential temperature gradient is reversed, and that forcing terms are used to drive the turbulence by adding kinetic energy to the velocity scalar. As a simple example, ODT simulations have been run by setting up a periodic domain with a stable potential temperature gradient g_o and applying a sinusoidal driving force with a specified wavelength Λ. These simulations are compared to stably stratified mixing experiments in which salt water with a constant initial salt concentration gradient (analogous to a potential temperature gradient) is stirred to generate turbulence.

The remarkable observation from these experiments, described in Ruddick, *et al.* (1989), Park, *et al.* (1994), and Holford & Linden (1999), is that the initially constant salt concentration gradient breaks up into a series of well-mixed layers separated by sharp conentration gradients. Although this phenomenon is most likely unique

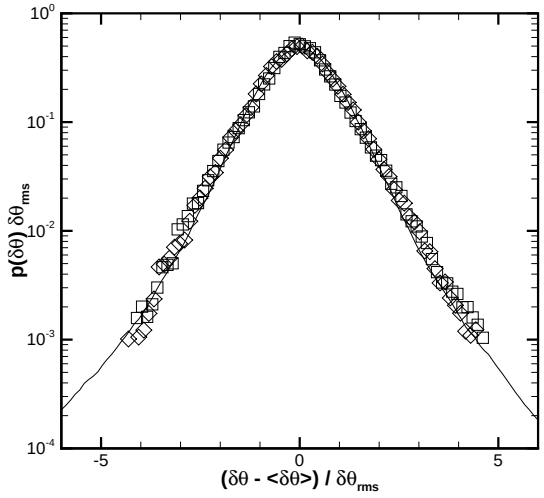

Figure 4: Rescaled probability p of a potential temperature fluctuation $\delta\theta$ (lines) for $Pr = 5.5$, $Ra = 2 \cdot 10^9$. Here $\langle\delta\theta\rangle = 0.5\Delta\theta$ and $\delta\theta^2_{rms}$ is the variance of the PDF. For comparison, experimental data in two distinct cell geometries (squares for cylindrical geometry, diamonds for rectangular geometry) with the same Ra and Pr are also shown (Daya & Ecke 2001).

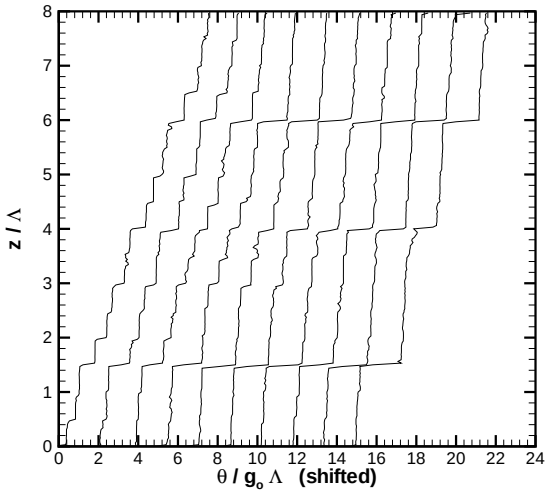

Figure 5: Potential temperature profiles, exhibiting spontaneous layer development in stably stratified turbulence.

to fluids with a high Prandtl (or Schmidt) number, and hence not directly applicable to the ABL, it still provides an interesting test of the ODT model. Details of the ODT simulations can be found in Wunsch & Kerstein (2001).

Figure 5 shows a series of potential temperature profiles (equivalent to salt concentration profiles in a salt water experiment) from ODT simulations with a Prandtl number of 100. The periodic domain has a height of 8Λ, so the potential temperature increases by $8g_o\Lambda$ across the domain. The leftmost profile is taken soon after the start of the simulation; subsequent profiles at later times are shifted to the right by $2g_o\Lambda$ for clarity. One can see that a number of small, transient mixed regions form initially and then merge to form three large, persistent layers. This behavior is qualitatively similar to the experimental observations in salt water tanks.

Absolute quantitative comparison with experiment is not possible, because the stirring mechanism in the ODT model is somewhat artificial and cannot be matched directly to the experimental stirring rod size and velocity. However, trends with the two dimensionless control parameters, the Richardson number Ri (stratification strength) and the Reynolds number Re (turbulence intensity) can be compared. Figure 6 shows a comparison of the layer sizes L between ODT data and the experiments of Park, *et al.* (1994). For this comparison, the ODT integral scale Λ was identified with the experimental stirring rod diameter. An arbitrary constant of proportionality between the ODT velocity scale and the stirring rod speed was introduced to help align the two data sets. Other values of this constant translate the ODT data across the figure but do not change the trend. The figure plots $Re^{1/4}\Lambda/L$ versus Ri because a simple scaling analysis (Wunsch 2000) suggests that $Re^{1/4}\Lambda/L$ should scale linearly with Ri. The ODT data strongly support this scaling, and the experimental data are also consistent with it (except for one outlier point).

It is remarkable that the same ODT model that was used to study Rayleigh-Beńard convection can reproduce this remarkable layering phenomenon in stably stratified turbulence. The model itself is not changed; only the physical inputs such as the forcings, boundary conditions, and fluid properties (Pr) differ for the two problems. This robustness is important for ABL work, since periods of both stable and unstable stratification occur over the course of a typical diurnal cycle.

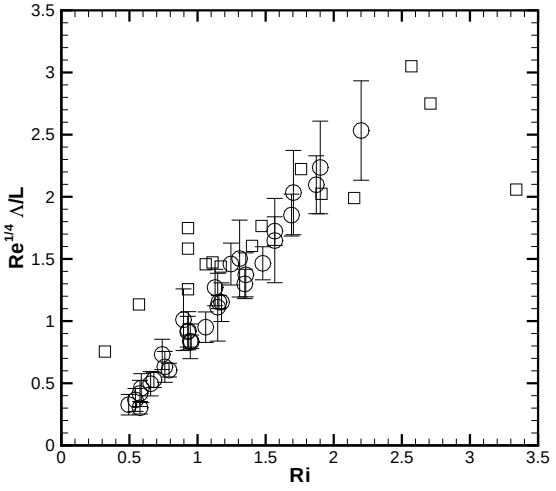

Figure 6: Ratio of layer size L to integral scale Λ as a function of Reynolds number (Re) and Richardson number Ri. Circles with errorbars are from ODT simulations; squares are from the salt water experiments of Park, *et al.* (1994).

3.3 CEI

The cloud-top entrainment instability (CEI) is a proposed mechanism for buoyant mixing at the top of a stratocumulus cloud (Randall, 1980; Deardorff, 1980). Since it involves regions of stable as well as unstable stratification, it provides a stringent test of the ODT model. Laboratory experiments by Shy & Breidenthal (1990) attempt to reproduce salient features of CEI in a simplified configuration. ODT simulations of these experiments have been used to quantitatively test the model in the presence of both stable and unstable stratifcation (Wunsch, 2003).

In the experiments of Shy & Breidenthal (1990), a two-fluid mixture was used, with the fluid density (and buoyancy) being a non-monotonic function of the mixture fraction χ. In the initial configuration, one pure fluid $(\chi = 1)$ with density ρ_t was placed above another fluid $(\chi = 0)$ with a greater density $\rho_t + \Delta\rho$. This configuration is stably stratified, except for the fact that mixtures of the two fluids have densities greater than either pure fluid; the maximum density of $\rho_t + D_o\Delta\rho$ occurs at a mixture fraction of χ_m. Mixing of the fluid at the interface therefore results in a region of unstable stratification, which drives further mixing and instability. The creation of unstable stratification from the initially stable stratification is dubbed 'buoyancy reversal.'

Figure 7 shows a series of density profiles from ODT simulation of this problem. In the initial (leftmost) profile, the pure high-density fluid lies below pure low-density fluid, with the mixture fraction increasing linearly from 0 to 1 betweem $z = 0.7\Lambda$ and $z = 0.8\Lambda$. The density maximum lies between these points, creating a small region of instability. At later times, the region of instability grows as convection mixes the fluid in the lower portion of the tank. The boundary between the two fluids becomes sharper in later profiles, and a little turbulent mixing is also seen on the stable side of the interface. These profiles are consistant with the qualitative observations of Shy & Breidenthal (1990).

To evaluate the state of the system at any given time, a buoyancy reversal parameter D based on the densities at the top $(z = \Lambda)$ and bottom $(z = 0)$ of the tank is defined as

$$D \equiv \frac{\rho(\chi_m) - \rho(z=0)}{\rho(z=0) - \rho(z=\Lambda)}. \qquad (13)$$

In the initial state, $D = D_o$ by construction. Shy & Breidenthal (1990) measured the value of D after about two minutes of turbulent convection for a range of values of D_o. Their results are compared with the ODT simulation results for the same parameter values in Figure 8. The agreement is very good.

The experiments of Shy & Breidenthal (1990) differ from CEI in the atmosphere in many respects. One of these is the Prandlt number (Pr), which is of order 1000 in the lab experiment but of order 1 in the atmosphere. ODT can be a valuable tool for exploring the significance of this (and other) differences between laboratory experiments and ABL physics. Figure 9 shows the value of D_f as a function of D_o for three different values of Pr. The impact of this parameter is quite pronounced.

4 ABL SIMULATIONS

Recently, the ODT model has been used to study the ABL in two basic configurations: unstable stratification (constant heating rate at the ground) and stable stratification (constant cooling rate at the ground). At the present time it is not economical to simulate the vertical air column up to a height of order one kilometer while

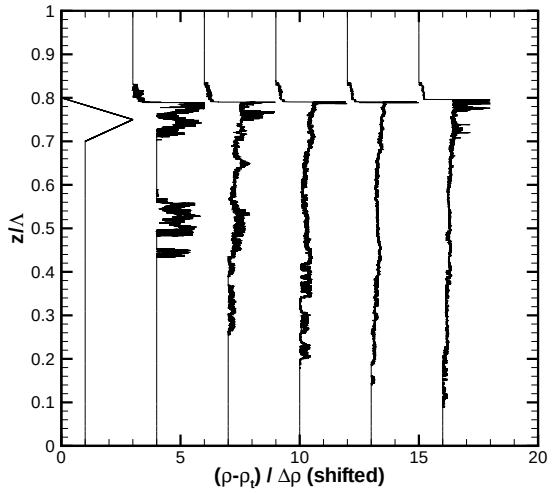

Figure 7: Density profiles, showing convective mixing below the fluid interface in a CEI simulation.

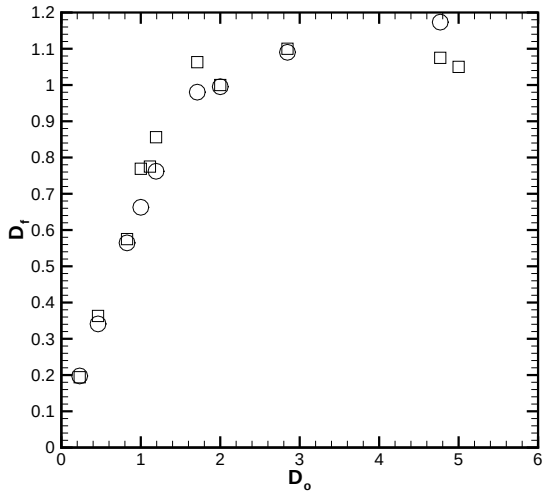

Figure 8: Final value of the buoyancy-reversal parameter after 2 minutes, as a function of the intial value D_o. Squares are data from the experiment of Shy & Breidenthal (1990); circles are corresponding ODT simulations.

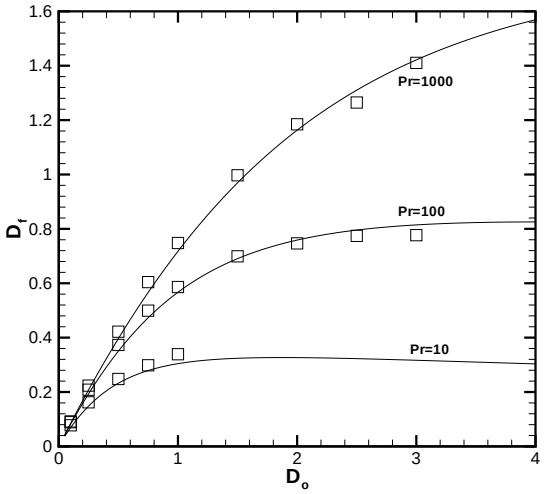

Figure 9: Final value of the buoyancy-reversal parameter as a function of D_o for three different Prandtl numbers. Squares are data from ODT simulations; lines are a theoretical model described in Wunsch (2003).

resolving the molecular scales, so the molecular transport parameters (ν and κ) were increased from their physical values by a factor of order 1000 for these simulations. Detailed study of ABL problems using ODT is just beginning, so quantitative comparisons of the type described in the previous section are not yet available. The purpose of this discussion is merely to show that ODT can at least qualitatively reproduce important features of the ABL.

A simple nocturnal (stable) boundary layer in the Arctic, described in Kosovic & Curry (2000), has been simulated using the ODT model. In this configuration, shear-driven turbulence results from a uniform geostrophic wind in a stably stratified boundary layer with a constant cooling rate at the ground. This case forms the basis for the GABLS SCM intercomparison study (Cuxart, *et al.* 2004), of which the ODT model is a participant. Additional details of the ODT simulations of this problem can be found in Kerstein & Wunsch (2004).

To illustrate the ODT results for the GABLS intercomparison case, figure 10 shows several potential temperature profiles from this simulation. Figure 11 demonstrates that ODT reproduces the Ekman spiral which results from the geostrophic wind. Both of these profiles are

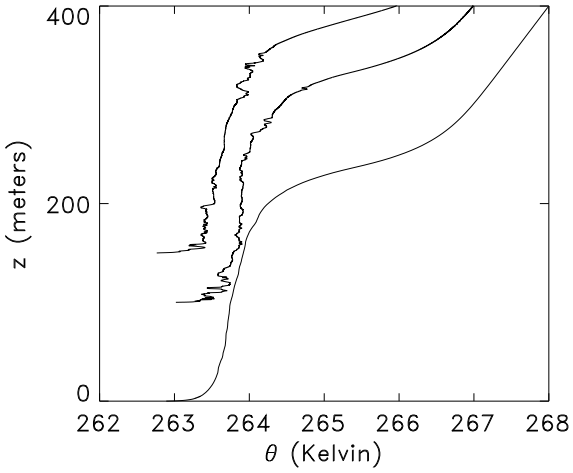

Figure 10: The vertical profile of the potential temperature (averaged over a one-hour interval) in the GABLS (stably stratified) ABL simulation. Also shown are two instantaneous potential temperature profiles, displaced upward by 100m and 150m, respectively.

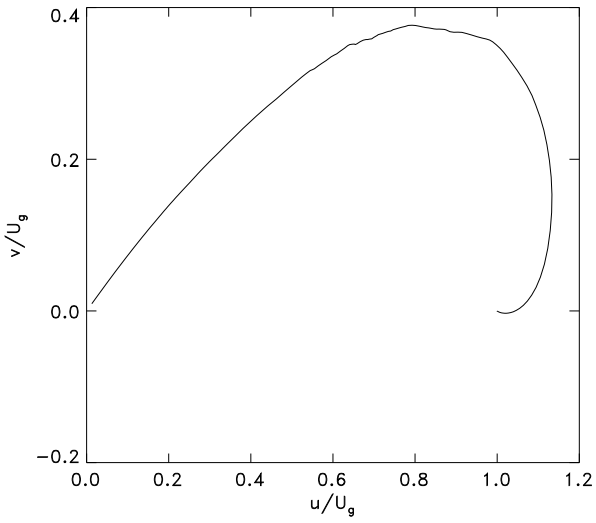

Figure 11: Normalized Ekman spiral, from the GABLS (stably stratified) simulation.

consistent with the LES results of Kosovic and Curry (2000) as well as LES results reported in the GABLS intercomparison.

A clear-air, windless, daytime (unstable) boundary layer problem, described in Sullivan, *et al.* (1998), has also been simulated using ODT. In this problem, the boundary layer consists of a neutrally stratified (constant potential temperature) region above the ground, capped by a region of stable stratification (potential temperature gradient). A constant heating rate applied to the ground causes unstable convection to occur there. This convection erodes the stable region. Figure 12 shows a series of potential temperature profiles from an ODT simulation of this configuration, with parameter values based on those in Sullivan, *et al.* (1998). As the simulation progresses, the mean potential temperature in the convecting region increases, and the convection penetrates into the stable region. These results are qualitatively similar to the LES data reported in Sullivan, *et al.* (1998). Quantitative comparison of the results is not yet complete.

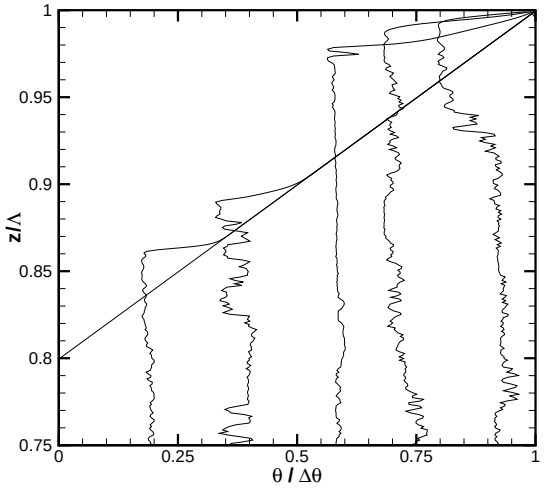

Figure 12: Potential temperature profiles (at 30 minute intervals), normalized by the total potential temperature increase $\Delta\theta$ across the domain, from the convective boundary layer simulation. The domain height is $\Lambda = 1500$m; the upper 300m ($z \geq 0.8\Lambda$) is stably stratified initially. As the lower region heats up, the convection erodes the stably stratified upper region.

5 FUTURE APPLICATIONS

There are a wide range of potential uses for the ODT model in studying the ABL. Several approaches are possible, with different goals and potential benefits. One of these is fully-resolved simulations of detailed physical processes in the ABL. In this approach, all microscopic processes are fully resolved, as was done for the experimental comparison studies discussed in section three. Due to the computational cost, it is not possible to simulate the full ABL with this approach at the present time. The goal of this approach would be to improve the understanding of small-scale physical processes in turbulent atmospheric flows, such as CEI or atmospheric chemistry problems. Another use of this approach is to help understand the connection between laboratory results and similar ABL flows which have different values of the governing parameters.

ODT may also be used to study the full ABL column in the same manner as a traditional SCM. In this case, it is not economical to fully resolve the smallest scales. Simple closure schemes, similar to those applied to LES, are being developed for this purpose (Kerstein & Wunsch, 2004). In spite of this need, the range of scales resolvable in ODT still exceeds what is currently feasible in LES by several orders of magnitude.

Finally, like other SCMs, ODT could be incorporated into LES simulations or GCM models to study regional or global atmospheric flows. The use of ODT as an LES subgrid model is already being explored (Kerstein, 2002; Schmidt, *et al.* 2003). Its unique feature relative to other SCMs is its formulation as an unsteady simulation of an individual flow realization rather than an evolution of ensemble-averaged properties. This offers possibilities such as realistic representation of time-lagged response to transients and avoidance of realizability problems. However, it remains to be demonstrated that ODT is in fact advantageous for subgrid closure of multi-dimensional ABL simulations.

6 ACKNOWLEDGEMENT

This research was supported by the Division of Chemical Sciences, Geosciences, and Energy Biosciences, Office of Basic Energy Sciences, U.S. Department of Energy.

References

[1] Ahlers, G. & Xu, X., 2001: Prandtl-number dependence of heat transport in turbulent Rayleigh-Beńard convection. *Phys. Rev. Lett.* **86**, 3320-3323.

[2] Ashurst, W., Kerstein, A.R., Wunsch, S., and Nilsen, V., 2001: One-dimensional turbulence: vector formulation and application to free shear flows. *J. Fluid Mech.* **447**, 85-109.

[3] Cioni, S., Ciliberto, S. & Sommeria, J., 1997: Strongly turbulent Rayleigh-Beńard convection in mercury: comparison with results at moderate Prandtl number. *J. Fluid Mech.* **335**, 111-140.

[4] Cuxart, J., et al., 2004: Single-column intercomparison for a stably stratified atmospheric boundary layer. Submitted to *Boundary Layer Meteorol.*.

[5] Daya, Z.A., & Ecke, R.E., 2001: Does turbulent convection feel the shape of the container? *Phys. Rev. Lett.* **87**, 184501.

[6] Deardorff, J.W., 1980: Clound-top entrainment instability. *J. Atmos. Sci* **37**, 131.

[7] Holford, J.M., & Linden, P.F., 1999: Turbulent mixing in a stratified fluid. *Dyn. Atmos. Oceans* **30**, 173.

[8] Kadanoff, L.P. 2001: Turbulent Heat Flow: Structures and Scaling. Physics Today, **54**(8), 34-39.

[9] Kerstein, A.R., 1991: Linear-eddy modeling of turbulent transport. Part 6. Microstructure of diffusive scalar mixing fields. *J. Fluid Mech.*, **231**, 361-394.

[10] Kerstein, A.R., 1999: One-dimensional turbulence, Formulation and application to homogeneous turbulence, shear flows, and buoyant stratified flows. *J. Fluid Mech.*, **392**, 277-334.

[11] Kerstein, A.R., 2002: One-dimensional turbulence, A new approach to high-fidelity subgrid closure of turbulent flow simulations. *Comp. Phys. Commun.*, **148**, 1-16.

[12] Kerstein, A.R., and Wunsch, S., 2004: Simulation of the GABLS stable boundary layer intercomparison case using One-Dimensional Turbulence. AMS 16th Symposium on Boundary Layers and Turbulence, Portland, Maine.

[13] Kosovic, B., and Curry, J., 2000: A large eddy simulation study of a quasy-steady, stably stratified atmospheric boundary layer. *J. Atmos. Sci.*, **57**, 1052-1068.

[14] Krueger, S.K., "Linear eddy modeling of entrainment and mixing in stratus clouds." *J. Atmos. Sci.*, **50**, 3078-3090 (1993).

[15] Niemela, J.J., Skrbek, L., Sreenivasan, K.R. & Donnelly, R.J., 2000: Turbulent convection at very high Rayleigh numbers. *Nature* **404**, 837-840.

[16] Park, Y., Whitehead, J.A., & Gnanadeskian, A., 1994: Turbulent mixing in stratified fluids: layer formation and energetics. *J. Fluid Mech.*, **279**, 279.

[17] Randall, D.A., 1980: Conditional instability of the first kind upside down. *J. Atmos. Sci.* **37** 125.

[18] Ruddick, B.R., McDougall, T.J., & Turner, T.S., 1989: The formation of layers in a uniformly stirred density gradient. *Deep-Sea Res.* , **36**, 597.

[19] Schmidt, R.C., Kerstein, A.R., Wunsch, S., and Nilsen, V., 2003: Near-wall LES closure based on one-dimensional turbulence modeling. *J. Comp. Phys.*, **186**, 3170-355.

[20] Shy, S., and Breidenthal, R., "Laboratory experiments on the cloud-top entrainment instability." *J. Fluid Mech.* **214**, 1-15 (1990).

[21] Stull, R.B., 1988: *An Introduction to Boundary Layer Meteorology*. Kluwer, Dordrecht.

[22] Su, C.-W., Krueger, S.K., McMurtry, P.A., and Austin, P.H., 1998: Linear eddy modeling of droplet spectral evolution during entrainment and mixing in cumulus clouds. *Atmos. Res.*, **47-48**, 41-58.

[23] Sullivan, P., Moeng, C.H., Lenschow, D., and Mayer, S., 1998: Structure of the entrainment zone capping the convective atmospheric boundary layer. *J. Atmos. Sci.* **55**, 3042-3064.

[24] Wunsch, S., 2000: Scaling laws for layer formation in stably stratified turbulence. *Phys. Fluids*, **12**, 672.

[25] Wunsch, S., and Kerstein, A.R., 2001: A model for layer formation in stably-stratified turbulence. *Phys. Fluids*, **13**, 702-712.

[26] Wunsch, S., 2003: Stochastic simulations of buoyancy-reversal experiments. *Phys. Fluids*, **15**, 1442-1456.

[27] Wunsch, S., and Kerstein, A.R., 2004: A stochastic model for high Rayleigh number convection. Submitted to *J. Fluid Mech.*

[28] Xia, K.-Q., Lam, S. & Zhou, S.-Q., 2002: Heat-flux measurement in high-Prandtl-number turbulence Rayleigh-Beńard convection. *Phys. Rev. Lett.* **88**, 064501.